Precision Engineering 52 (2018) 266–275

Contents lists available at ScienceDirect

Precision Engineering

journal homepage: www.elsevier.com/locate/precision

Superhydrophobic structures on 316L stainless steel surfaces machined by nanosecond pulsed laser

Yukui Cai[a], Wenlong Chang[a], Xichun Luo[a,*], Ana M.L. Sousa[b], King Hang Aaron Lau[b], Yi Qin[a]

[a] Centre for Precision Manufacturing, DMEM, University of Strathclyde, UK
[b] WestCHEM/Department of Pure & Applied Chemistry, University of Strathclyde, UK

ARTICLE INFO

Keywords:
Superhydrophobic surface
316L stainless steel
Nano-second pulse laser
Surface structuring

ABSTRACT

In this paper nanosecond laser machining process was developed to improve the hydrophobicity of AISI 316L stainless steel surface. A geometrical model of laser machined Gaussian micro hole, together with constrain conditions, was established for the first time to predict surface contact angle and optimize structure geometries for maximizing its hydrophobicity. The effects of processing laser power and pitch of microstructures on the topography of the machined surface were investigated through laser machining experiment. Subsequently, the water droplet contact angle was measured to evaluate the hydrophobicity of different specimens. Results show that under the laser power of 10 W and 14 W, with the increase of the pitch of microstructures, the contact angle increases until it reaches its peak value then drops gradually. Under the large pitch of microstructure, the contact angle will increase with the increase of the processing laser power. Under the same pitch of microstructure, the contact angle will increase with the increase of ten-point height of surface topography, Sz which is a better parameter than Sa (arithmetical mean height) to characterise hydrophobicity of surface with Gaussian holes. This study shows that large Sz is an essential condition to form the stable and robust Cassie–Baxter state, i.e. a condition to achieve superhydrophobicity. The comparison between the predicted and measured contact angles in experiments shows that the proposed model can accurately predict contact angle and optimize the geometries of the microstructure to achieve maximum hydrophobicity.

1. Introduction

Superhydrophobic surfaces have recently received tremendous attention because of special functions such as self-cleaning, corrosion protection, anti-icing, drag reduction and anti-bacteria offered by them [1–6]. Surfaces with water contact angle greater than 150° are generally classified as superhydrophobic surfaces. Many creatures in nature, including the lotus leaf [7], rice leaf [8], butterflying wing [9] and water-strider legs [10] exhibit excellent superhydrophobicity.

Previous researches show that surface coating to reduce surface free energy and fabrication of surface structures are two important methods to achieve superhydrophobic surface [11]. Many approaches for the preparation of superhydrophobic surfaces have been put forward over the last decade, such as electrochemical deposition [12], plasma method [13], chemical vapour deposition [14], wet chemical reaction [15], sol-gel processing [16], lithography [17], electrospinning [18], solution immersion [19], micro milling [20,21], laser machining [22,23] etc. Many surfaces manufactured by chemical methods have good superhydrophobicity but low stability and service life. The major challenges for industrial application of superhydrophobic surface are low production efficiency and high production cost. Instead, laser machining is a reliable manufacturing method due to its high-efficiency and contactless characteristics. Until now, most of laser texturing works use expensive femtosecond or picosecond pulse lasers [24,25]. Many researchers reported that hierarchical structures generated in femtosecond or picosecond pulse laser machining process that consists of micron and nanoscale level pattern is a critical condition for improving surface hydrophobicity [26–28].

Nanosecond laser machining has been proved to be a very promising cost-effective method for surface texturing. Several researchers have paid attention to the study of hydrophobic metal structures machined by using nanosecond laser [23,29–31]. Razi and co-workers carried out research on wettability control on stainless steel by nanosecond laser surface texturing [32–34]. They investigated the surface morphology, surface oxygen content and wettability of specimens machined in air and water [32]. The results showed that the specimen treated in the air has large surface structures than the specimen treated in water [32]. More importantly, they also found a remarkable change from

* Corresponding author.
E-mail address: xichun.luo@strath.ac.uk (X. Luo).

https://doi.org/10.1016/j.precisioneng.2018.01.004
Received 6 October 2017; Received in revised form 26 November 2017; Accepted 6 January 2018
Available online 08 January 2018

hydrophilicity to hydrophobicity after 10 days exposed to ambient air [34]. Duong [23] demonstrated wetting behaviour on nanosecond laser patterned copper and brass surfaces, with the static contact angle of up to 152°. Jagdheesh [29] created near superhydrophobic surface with a maximum contact angle of 148° by using one-step direct laser writing technique. The results show that the micro-holes and the formation of micro-wall play a major role compared with surface chemical change for improving superhydrophobicity. Yang [30] modified the wetting property of Inconel 718 by nanosecond laser machining approach and the maximum contact angle of 156° was obtained. Kwon [31] proposed a sequential fabrication process for a superhydrophobic stainless steel surface, combined with laser machining and electrodeposition, the maximum contact angle obtained was 153°. However, no research has yet been conducted to build a theoretical model used for structure design based on nanosecond laser machining characteristic. The constrained conditions for a stable Cassie-Baxter state superhydrophobic are still not clarified.

AISI316L stainless steel has been widely used for biomedical implants and surgical instruments, such as hemostat, surgical knives and dental devices. Several studies have been conducted on the superhydrophobicity of 316L stainless steel [11,35]. Chen [11] fabricated the reed leaf-like superhydrophobic structures on stainless steel by nanosecond laser cutting, and the maximum apparent contact angle reached 157°. Trdan [35] reported the wettability modulation from superhydrophilic to superhydrophobic surface state on corrosion behaviour of 316L fabricated by YAG nanosecond direct laser texturing technique. The corrosion resistance test results indicate that the superhydrophobic surface has improved passivation ability and lowest corrosion current density. Thus, superhydrophobicity of 316L is intimately related to its practical application. However, the effects of laser power and structure pitch on surface topography of 316L stainless steel still need further research. In addition, the effects of dimension of structure and surface roughness related evaluation parameter on hydrophobicity of specimen are still unclear.

The above literature shows that nanosecond laser machining is a promising method for manufacturing superhydrophobic structures on 316L stainless steel. However, there are still many challenges need to be further researched. First of all, geometrical model and theoretical analysis of hydrophobicity for laser machined surface need to be established to assist the prediction of contact angle and structure design. Moreover, the mechanism of influence of laser power on 316L stainless steel topography and its superhydrophobicity still requires further research. Besides, the dimension of structure and its effect on hydrophobicity are still unclear.

In this research, we present a high-efficiency and easily-controlled method for manufacturing superhydrophobic surfaces using a nanosecond laser. This work is an attempt to investigate the effects of micro hole structures on hydrophobicity of 316L stainless steel obtained by nanosecond laser under different laser powers. Firstly, the geometrical model based on laser machining Gaussian holes will be built. Moreover, theoretical analysis of the constraints for a superhydrophobic surface will be carried out to explain what kinds of dimension can promote larger contact angle and make the droplet have a stable Cassie-Baxter state on the specimen surface. Then, the micro holes with various pitches will be fabricated on the specimens under various laser powers. The influence of laser power and various pitches on the machined surface roughness will be discussed after surface measurement by SEM and optical microscope. Finally, the measured static contact angle and structure dimensions were compared with predicted values in order to validate and evaluate the prediction model.

2. Prediction model for contact angle based on characteristics of micro Gaussian hole

Our major purpose is to obtain the stainless steel specimen possessing good superhydrophobicity, which means that the droplet should have a stable Cassie-Baxter state on the specimen surface. Thus, in this section, the mechanism of superhydrophobicity will be studied from the theoretical point of view. Moreover, the condition of stable and robust Cassie-Baxter state droplet will also be investigated.

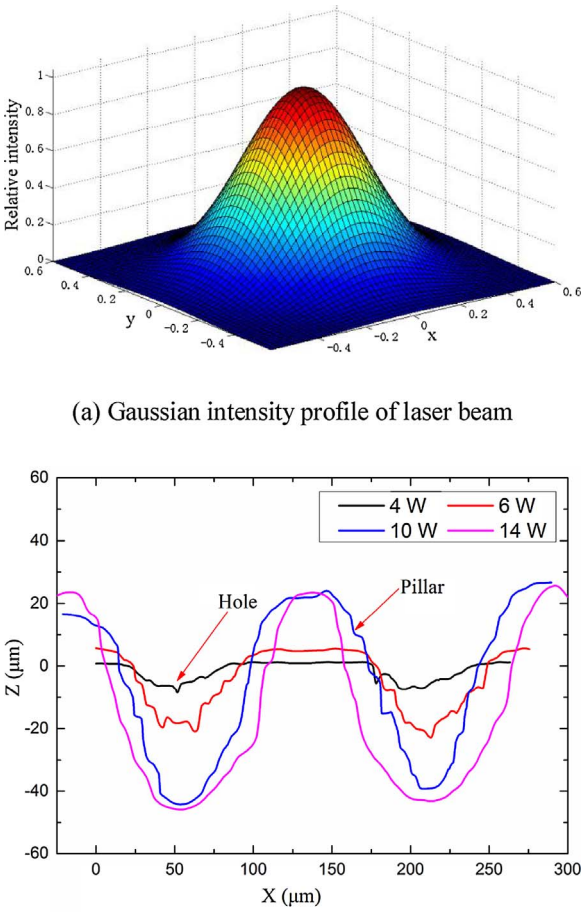

(a) Gaussian intensity profile of laser beam

(b) Surface profile for P110 arrays

Fig. 1. Surface profiles of nanosecond laser beam and machined micro holes.

The nanosecond laser beam has a Gaussian intensity profile as shown in Fig. 1(a), so the profile of laser machined micro hole will be also like a Gaussian curve. In order to investigate the effect of laser power on the surface topography of micro hole, some micro holes with pitch of 110 μm (P110) are machined at different laser powers on stainless steel specimens. Then the surface topography of specimen was measured by an optical microscope (Alicona G4) under 50X Magnification objective. This instrument has a vertical resolution of 20 nm. The surface profiles extracted along the diagonal direction of the machined holes under different laser powers for P110 are shown in Fig. 1(b). The depth and the width of the micro holes are observed to increase in proportion to the laser power. Especially, when the laser power varies from 4 W to 14 W, the average depth of the micro holes gradually increases from 9.2 μm to 68.3 μm. Besides, it also leads to the increase of the height of pillars and decrease of the width of the pillars from 90 μm to 30 μm. The depths of the micro holes are almost the same at 10 W and 14 W, but the pillar width will further decrease as the increase of laser power leads to more materials removed from the specimen surface.

2D profile of micro hole can be described by Gaussian function as shown in Eqs. (1) and (2). For the Gaussian curve, the proportion of area occupied between −3c and +3c is about 99.7%, so the curve between ± 3c was chosen to represent the Gaussian hole machined by pulsed laser.

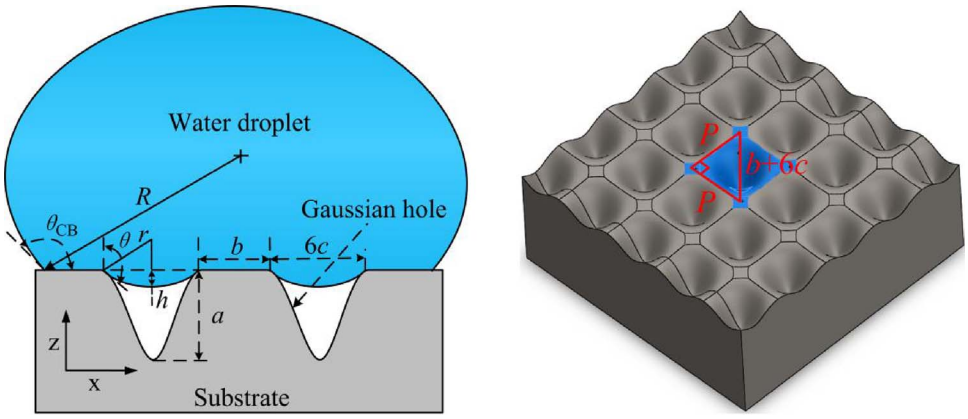

(a) 2D geometric model

(b) 3D topography

Fig. 2. Geometrical model of laser machined Gaussian holes at Cassie-Baxter state.

$$z = -a^{*}e^{-\frac{x^2}{2c^2}} \tag{1}$$

$$z = -a^{*}e^{-\frac{x^2+y^2}{2c^2}} \tag{2}$$

Where a and c are arbitrary real constants. The 2D and 3D geometrical models of laser machined Gaussian holes can be plotted based on Eqs. (1) and (2) and shown in Fig. 2. For a stable Cassie-Baxter state water droplet, it will have a little sag between micro pillars but cannot touch the bottom of micro holes [36,37]. In Fig. 2(a), a is the depth of the Gaussian hole, b is the width of micro pillar, $6c$ is the width of micro hole, h is the sag in height of droplet between pillars, θ is the intrinsic contact angle of stainless steel. We suppose that the sag of droplet surface is a ball surface and r is the ball radius. The 3D model based on Gaussian hole characteristic is shown in Fig. 2(b). The pitch P and b, c forms a right-angled triangle.

The surface contact angle at Cassie-Baxter state can be expressed as Eq. (3) [38]:

$$\cos\theta_{CB} = -1 + f(1 + \cos\theta) \tag{3}$$

where f is the fraction of solid surface area wet by the liquid and can be described as:

$$f = \frac{\text{actual conatct area}}{\text{planar area}} = \frac{b^2}{2\left(\frac{b}{2} + 3c\right)^2} \tag{4}$$

From Eqs. (3) and (4), it can be seen that the minimum value of f will help the contact angle θ_{CB} reach its maximum value.

In order to make the droplet keep a stable Cassie-Baxter state on the surface, the structure should meet some mathematical and chemical constraints which are listed as follows.

First of all, the droplet cannot contact with the bottom of the micro Gaussian hole, so the sag in height h should be smaller than a, which can be expressed as Eq. (5).

$$a > h = 3c\left(\frac{1-\sin\theta}{-\cos\theta}\right) \tag{5}$$

Eq. (5) can be further simplified as:

$$3c\left(\frac{1-\sin\theta}{-\cos\theta}\right) - a \le 0 \tag{6}$$

Secondly, the state of the droplet is affected by gravity and Laplace pressure (F) force. The Laplace pressure is the pressure difference between the inside and the outside of a curved surface that forms the boundary between a gas region and a liquid region [39]. The pressure difference is caused by the surface tension of the interface between liquid and gas. Thus, the balance between weight (W) and Laplace pressure (F) is also an essential condition for Cassie-Baxter state. It means that the Laplace pressure should be greater than weight (W) of the droplet. The average droplet weight for every hole and the Laplace pressure (F) are shown in Eqs. (7) and (8). The constraint can be expressed by Eq. (9). The pillar can be estimated to possess rectangular shape with side length b.

$$W = \frac{\rho\left(\frac{4}{3}\pi R^3 g\right)}{\pi R^2 \sin^2\theta}\left[2\left(\frac{b}{2} + 3c\right)^2 - b^2\right] \tag{7}$$

$$F = 12\pi\gamma_{lg}c\left(\frac{1-\sin\theta}{-\cos\theta}\right) \tag{8}$$

$$W - F \le 0 \tag{9}$$

where, γ_{lg} is the surface tension between liquid and gas.

Thirdly, the principle of the lowest energy is a general rule in nature. Since the mechanical system is trying to find a state of minimum surface free energy [40], the surface free energy of Cassie-Baxter state (E_{CB}) should be smaller than Wenzel state (E_W) [41]. The E_{CB} and E_W are calculated by Eqs. (10) and (11). The Eq. (12) is Young's equation [42]. The constraint about the principle of the lowest energy can be expressed by Eq. (13). The pillar side area is processed as a frustum of a pyramid to calculate the area.

$$E_{CB} = \gamma_{lg}\left[\frac{18\pi c^2(1-\sin\theta)}{\cos^2\theta}\right] + \gamma_{sl}b^2 + 4\gamma_{sg}\sqrt{a^2+9c^2}(b+3c) \tag{10}$$

$$E_W = \gamma_{sl}\left[b^2 + 4\sqrt{a^2+9c^2}(b+3c)\right] \tag{11}$$

$$\gamma_{sg} = \gamma_{lg}\cos\theta + \gamma_{sl} \tag{12}$$

$$E_{CB} - E_W \le 0 \tag{13}$$

Where γ_{sl} is the surface tension between solid and liquid, γ_{sg} is the surface tension between solid and gas.

Finally, there are some additional geometrical constraints, as shown in Fig. 2(b) according to the Pythagorean theorem, the relationship of b, c and P can be expressed as:

$$b + 6c = \sqrt{2}P \tag{14}$$

For every specimen, the depth of micro hole is also limited by actual depth. As an extension of Ra (arithmetical mean height of a line) to a surface, Sa is often used to evaluate surface roughness in an area. It represents the difference in height of each point compared to the arithmetical mean of the surface, so it cannot completely reflect the size of peak and valley on the periodic surface. On the other hand, the maximum height Sz is a surface characterisation parameter to evaluate the absolute highest and lowest points found on the surface, which is the sum of the maximum peak height (Sp) and the maximum valley depth (Sv) within the defined area. For this reason, Sz can reflect the

Table 1
Parameters used in the optimization.

θ (°)	R (mm)	γ_{lg} (N/m)
105	1.06	0.073

Table 2
Predicted dimensions of microstructures.

		P050	P070	P090	P110	P130	P150
Predicted dimensions (μm)	a	51.7	69	76.4	86	99.6	110.9
	b	13.8	20.6	31	40.8	49.1	58.3
	c	9.5	13.1	16	19.1	22.4	25.6
	$b/6c$	0.242	0.262	0.323	0.356	0.364	0.379
Predicted value of maximum θ_{CB} (°)		160.5	159.4	155.7	153.8	153.4	152.6

depth information of the specimen better than Sa. The depth of the hole should be smaller than Sz as shown in Eq. (15).

$$a \leq Sz \tag{15}$$

In this optimization problem, Eqs. (6), (14) and (15) are linear constraints while Eqs. (9) and (13) are nonlinear constraints. MATLAB Optimization Toolbox was used to solve the above optimization problems and the parameters in this study are listed in Table 1.

The predicted dimensions of a, b and c for 6 different pitches and the corresponding predicted maximum contact angles are shown in Table 2. With the increase of pitch from 50 μm to 150 μm, the ratio of b and $6c$ increased from 0.242 to 0.379. This means that it needs more solid part on the surface to sustain the water droplet to satisfy the constrained conditions, the droplet has a stable Cassie-Baxter state on the specimen surface. However, the increase of the ratio of b and $6c$ also results in decrease of the predicted maximum contact angle from 160.5° to 152.6°.

3. Pattern design and experimental details

The micro patterned surface of stainless steel was produced through laser ablation to verify the predicted structure dimension and contact angle. In addition, the effects of laser power and pitch on hydrophobicity of specimens will also be studied.

3.1. Material details and pattern design

Six AISI 316L stainless steel (Goodfellow Ltd.) specimens are used in this research. Each specimen has a dimension of 10 mm × 10 mm × 2 mm. Before laser machining, the specimens were plane milled using a 6 mm diameter end mill to ensure the surfaces are smooth. The machined surface roughness Sa and Sz are 0.2 μm and 2.1 μm respectively after milling operations.

Micro-holes arrays designed for this experiment is shown in Fig. 3. P is the pitch between two adjacent holes. As listed in Table 3, the pitch (P) varies from 50 μm to 150 μm for the six specimens. But for each specimen, the pitches are the same in the vertical and horizontal directions.

3.2. Experimental setup

The laser machining experiments will be carried out on a hybrid ultra-precision machine shown in Fig. 4. It is equipped with a nanosecond pulsed fiber laser which has central emission wavelength of 1064 nm. The laser source has a nominal average output power of 20 W and its maximum pulse repetition rate is 200 kHz. For a pulse repetition rate of 20 kHz, the average pulse duration is 100 ns and pulse energy is 1 mJ. Achromatic doublet with a focal length 26.054 mm was used to

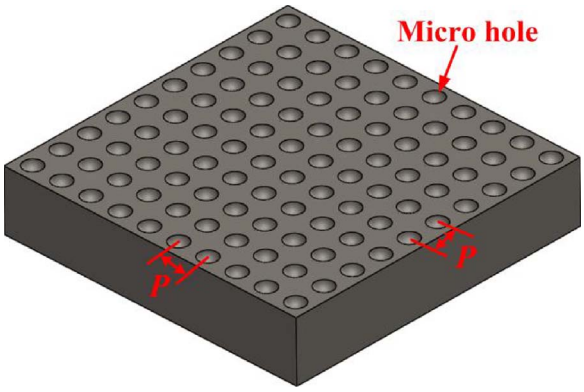

Fig. 3. Schematic of micro hole array.

Table 3
Pitches for different specimens.

Pattern type	P (μm)
Hole array	50, 70, 90, 110, 130, 150

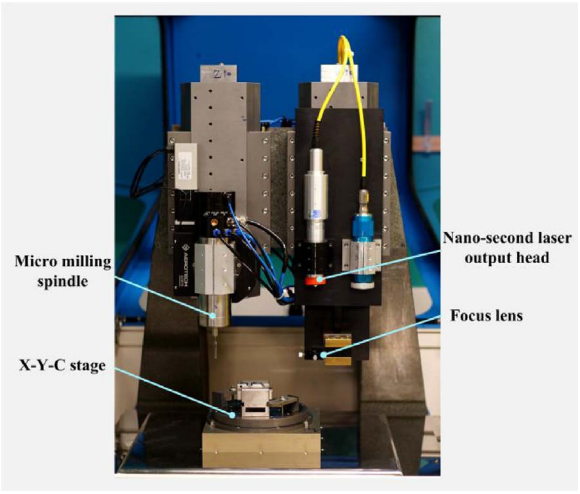

Fig. 4. Hybrid ultraprecision machine.

Table 4
The laser cutting parameters in the experiments.

Laser power (W)	Pulse repetition rate	Feed rate (mm/min)	Duration time (S)
4, 6, 10, 14	100 K	200	0.4 S

focus laser pulse. The achieved spot size is about 15 um diameter. During operation, the laser beam passes through a lens and focuses onto the specimen surface which is mounted on a precision X-Y-C stage. The laser machining parameters are listed in Table 4. The average laser power varies from 4 W to 14 W.

3.3. Post-processing

After laser machining, the specimens were rinsed with deionized water in ultrasonic cleaning equipment for half an hour to remove the molten slag on the surface. Then, these specimens were degreased in a 30-min ultrasonic bath in acetone and ethanol respectively. Finally, these specimens were dried in an oven. Before measuring the contact angle, these specimens were silanized in a vacuum oven using silane

reagent (1H, 1H, 2H, 2H-Perfluorooctyltriethoxysilane, 97%, Alfa Aesar Ltd), at 100 °C for 12 h to reduce their surface free energies.

3.4. Surface measurement and characterization method

The morphology of the laser structured surface was measured by a scanning electron microscope (SEM). Surface topography was measured by an optical 3D surface measurement device (Alicona G4). Apparent contact angle on surfaces was measured by a drop shape analyser (Kruss Ltd.) The selected water droplet volume was 5 μL. For each specimen, the apparent contact angle of the water droplet was measured three times and the average value was adopted.

4. Results and discussion

4.1. Analysis of surface morphology

Laser machining is a localized thermal process. The partial laser beam energy is absorbed by the material and resulting in material softening, local yielding, melting, burning or evaporation. The surface topography and dimensions of the machined structures vary with the laser power and the designed pitch. The SEM images of surface topography of P110 series specimens are shown in Fig. 5. It can be seen that the micro holes are well separated when the laser power is 4W. With the increase of laser power, a large amount of materials melted, the wall thickness between holes is reduced gradually. Then, the recast layer is formed on the circumference of the micro holes. The micro holes are partially overlapped each other as the wall materials melting and evaporation and formation of pillars gradually. Moreover, the pillar width decreases with the increase of laser power.

The SEM images of specimens machined under laser power of 14W for micro holes of different pitches are shown in Fig. 6. For a small pitch of 50 μm, the machined surface was ablated (as shown in Fig. 6(a)) due to large proportion of overlapping area. With the increase of pitch, the proportion of un-ablated surface increases and it starts to form rectangle pillars between holes gradually, as shown in Fig. 6(b), (c) and (d).

Fig. 7 shows the 3D surface morphologies of machined surfaces with pitch of 130 μm. It can be seen that only few materials are redeposited around the micro holes when using small laser powers of 4 W and 6 W, but some materials are deposited at the center of holes due to weak evaporations. With the increase of laser power, the depth and diameter of the holes are increased significantly and more and more molten material is deposited on the surface between micro holes. Especially, when laser power reaches 14 W, as shown in Fig. 7(d), the large volume of molten materials almost cover the whole surface between micro holes, which results in a rough surface and periodic pillar structures.

It has been recognized that the surface roughness has a significant effect on the hydrophobicity of the surface. The measurement results of surface roughness (Sz) are shown in Fig. 8. It can be seen that under the same pitch Sz increases with the increase of laser power for most specimens. The variation of Sz with laser power increases from 4 W to 14 W becomes more and more apparent with the increase of pitch. Especially, for the P050 specimen, the Sz increases from 31 μm to 51.7 μm. As the pitch increases from 50 μm to 150 μm, the Sz increases from 17.9 μm to 110.9 μm. Thus, with the increase of pitch, the gap of Sz becomes more and more significantly. The increase of pitch results in the increase of Sz value at higher laser power. The major reason is that higher laser power leads to more materials removed from the specimen surface and the increase of the depth of holes. Moreover, large pitch provides more space between holes for materials melt and lead to the increase of height of the recast layer.

However, it doesn't mean that the higher the laser power the higher the surface roughness is. The Sz value is also affected by the pitch. For

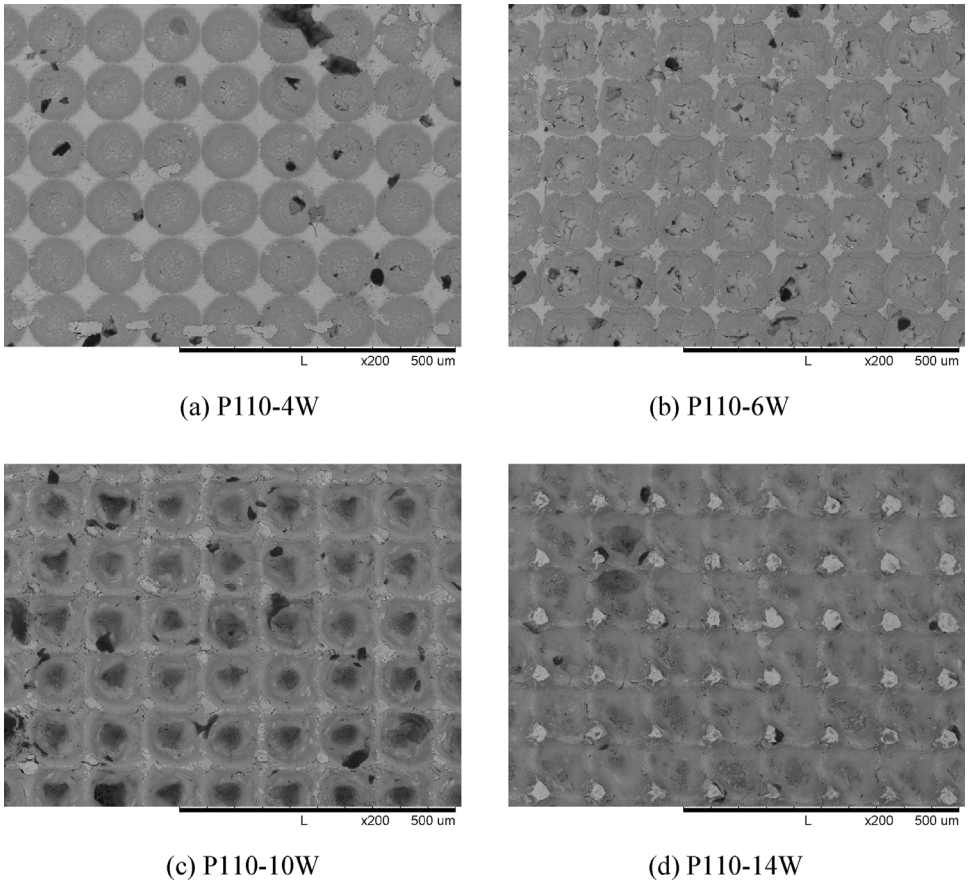

(a) P110-4W (b) P110-6W

(c) P110-10W (d) P110-14W

Fig. 5. SEM images of P110 specimens.

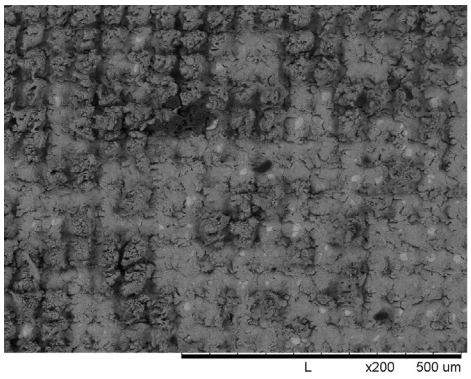

(a) P050-14W (50 μm pitch)

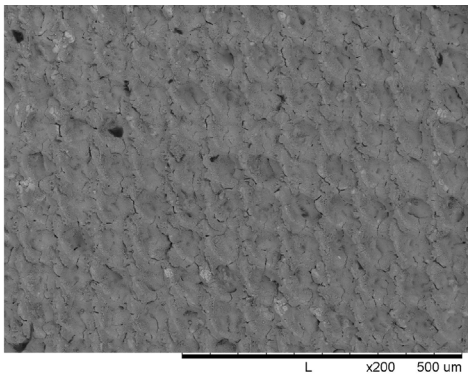

(b) P070-14W (70 μm pitch)

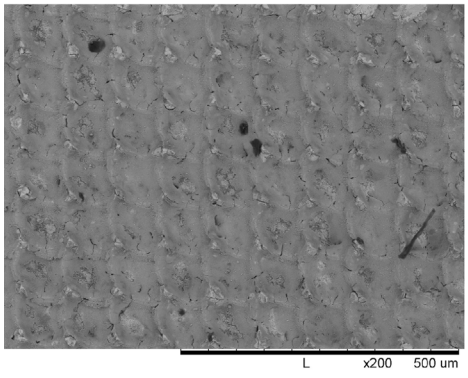

(c) P090-14W (90 μm pitch)

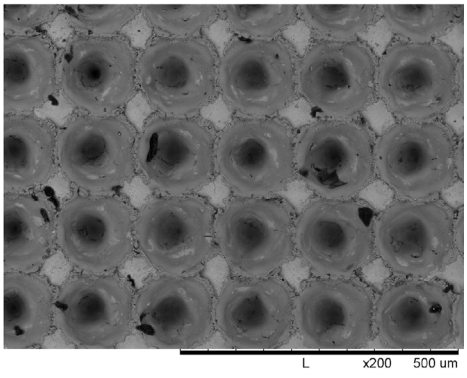

(d) P150-14W (150 μm pitch)

Fig. 6. SEM images of specimens machined under laser power of 14W.

specimen machined at the laser power of 4 W, the specimen P050–4 W has the maximum Sz value which is 43.5 μm. With the increase of pitch, the ratio of the un-ablated area increases, the interaction effect between the adjacent holes is weakened and leads to the decrease of surface roughness value. Under the high laser power of 10W and 14 W, the surface roughness Sz increases gradually with the increase of micro-structure pitch. The Sz value increases from 30.9 μm to 88.6 μm for laser power 10W series. As for laser power 14W series, the Sz value varies from 45.5 μm to 110.9 μm. With the increase of pitch, there is more space for un-treated surface which can deposit molten material. Thus, the height of pillar and the depth of holes will increase and lead to larger Sz value. However, for the small pitch specimen, there are untreated areas between holes, so the molten materials deposit on the ablated area. Consequently, the pillar height of the specimen with small pitch is lower than the large one.

In addition, under the same pitch, the surface roughness of some specimens machined under laser powers of 6 W or 10 W have larger Sz than the specimen machined under the laser power of 14 W. This phenomenon will affect the surface contact angle which will be discussed later. Especially, for specimen P050-6W, when laser power is 6 W, the machined surface has the maximum Sz value. For large laser power 10 W and 14 W, it will enhance the interaction effect between the holes and lead to the reduction of un-treated area and decrease of surface roughness Sz value. Thus, the surface roughness does not only influenced by the laser power, but also the pitch of micro holes. For every pitch, there is a corresponding laser power leads to maximum Sz. Moreover, with the increase of pitch of micro holes, the value of laser power should be higher in general.

4.2. Analysis of surface hydrophobicity

In this study, static contact angles of water droplet were measured using the sessile drop method to characterize hydrophobicity of the specimen surfaces, including a smoothly milled surface as a bench mark. A 5 μL droplet of deionised water was dropped on the smoothly milled specimen at atmospheric condition. The side view was captured by an industrial camera and the contact angle can be determined by image processing software on a PC. As shown in Fig. 9, the contact angle θ is 105° for the smoothly milled specimen.

4.2.1. Effect of laser power and pitch of structure on surface hydrophobicity

Fig. 10 shows the captured image of the droplets in the contact angle measurements. As shown in Fig. 10(d)–(f), the three specimens, P110–14 W (i.e. pitch of 110 μm under laser power of 14 W), P090–10 W and P050–6 W have the largest contact angles. In addition, compared with Fig. 9, with chemical treatments the contact angle of stainless steel surface is only 105°. It is laser structuring that further improves its hydrophobicity to 153.2°, which can be called super-hydrophobic surface.

Fig. 11 shows the variation of surface contact angle of the micro structured surface as a function of pitch and processing laser power. The error bar in the figure represents the minimum and maximum contact angle in three measurements for each specimen.

The micro structured surface machined at 4W has the same level of surface contact angle as smoothly milled surface of about 105°. As shown in Figs. Figure 5(a) and Figure 7(a), there are few materials were removed from specimens at the laser power of 4W. So the water droplet will entirely wet the structures and results in a homogeneous liquid-

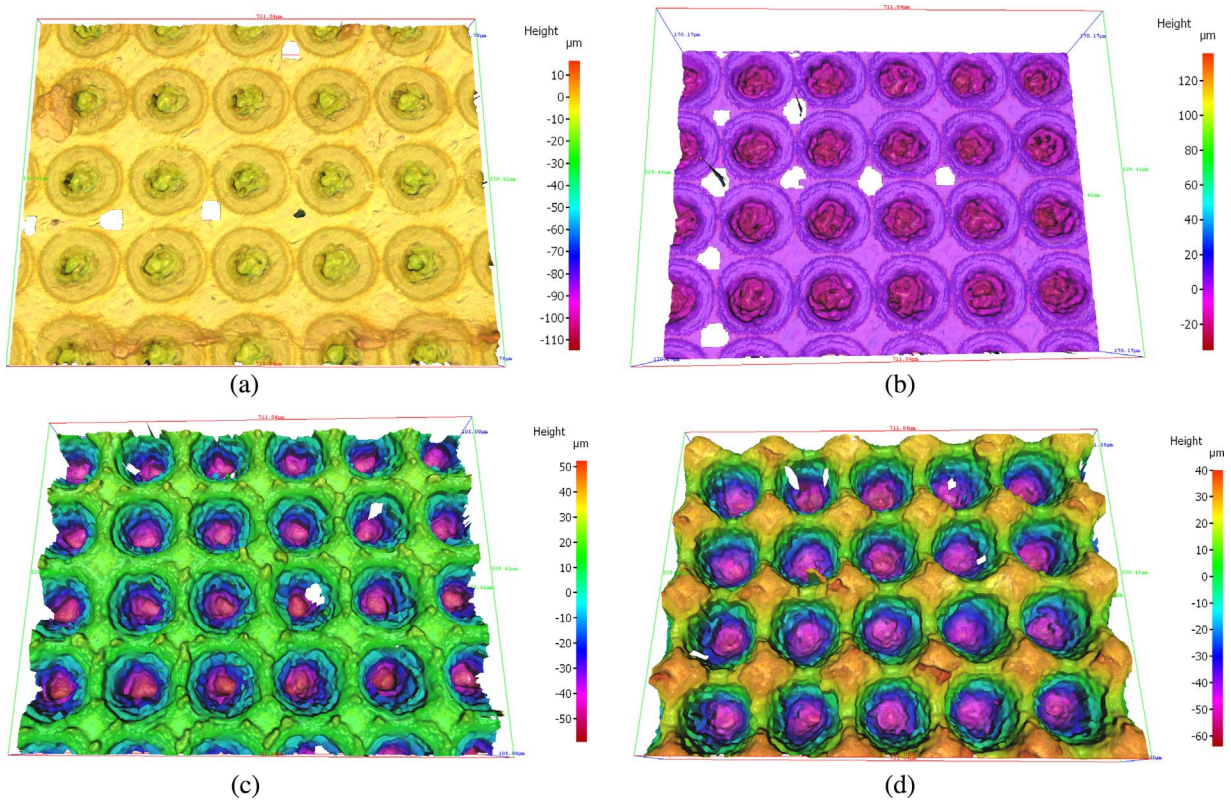

Fig. 7. Surface morphologies under different laser power for microstructures with different pitches (P130).

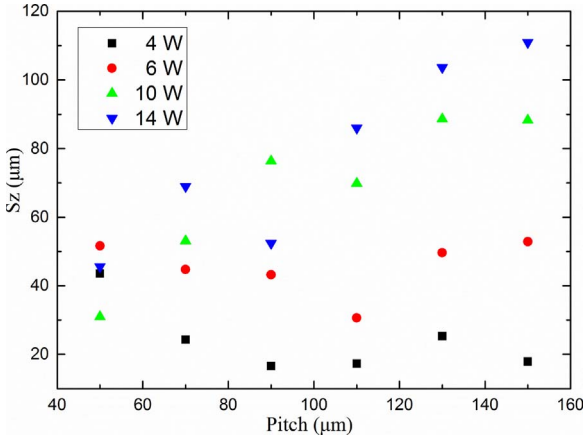

Fig. 8. Surface roughness of different laser power for micro hole arrays.

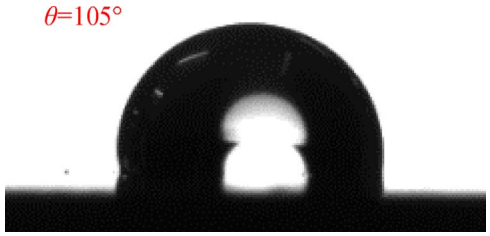

Fig. 9. Water droplet on the smoothly milled surface.

solid interface as described in Wenzel model. In addition, the surface contact angle decreases slightly when the pitch is chosen as 130 μm or 150 μm because Wenzel state becomes dominant.

For the specimens machined under the laser power at 6W, its contact angle shows a trend of gradual decrease. For the specimens machined under the laser powers at 10 W and 14 W, the trends of variation of the surface contact angle are very similar. With the increase of pitch, the contact angle rises up to a peak value and then gradually decreases. Moreover, with the increase of laser power, the pitch of specimen with peak value of contact angle increases gradually. In particular, for laser power of 6 W series, the maximum contact angle is 144.7° when the pitch is 50 μm. In addition, for laser power of 10 W, the maximum contact angle is 145.2° when the pitch is 90 μm. P110–14 W specimen has the best hydrophobicity among all specimens with contact angle of 153.2°, which can be classified as superhydrophobic surface. The above phenomenon can be explained as follows. Under the laser power of 6W, it has fewer materials removed from the specimen than 10W and 14W. Thus, with the crease of laser power, the width of micro hole 6*c* will also increase. The width of micro pillar *b* also needs increase in order to satisfy the constraints in Section 2. Otherwise, the state of water droplet will change to Wenzel state and leads to the reduction of contact angle. According to Eq. (14), the pitch with maximum contact angle will increase with the laser power. Consequently, the surface contact angle is not only affected by the laser power but also the microstructure pitch. With the increase of laser power, the best pitch, which has the maximum contact angle in the same laser power series, increasing from 50 μm to 110 μm.

The above analysis suggests that both the processing laser power and microstructure pitch have significant influences on the hydrophobicity of 316L stainless steel specimens. The influence of laser power on the surface contact angle is actually through surface roughness (Sz). As shown in Fig. 12 the increase of surface roughness Sz leads to the increase of contact angle under all machined pitches in this study. This can be explained as follows: the droplet can touch the bottom of the hole and shows Wenzel state when Sz is too small. Moreover, for the specimen with small Sz, even the droplet can stay as Cassie-Baxter state, due to minor space for air pocket under water droplet, the stability of Cassie-Baxter state is worse and easily transformed to Wenzel state. However, with the increase of Sz, the depth from peak to valley

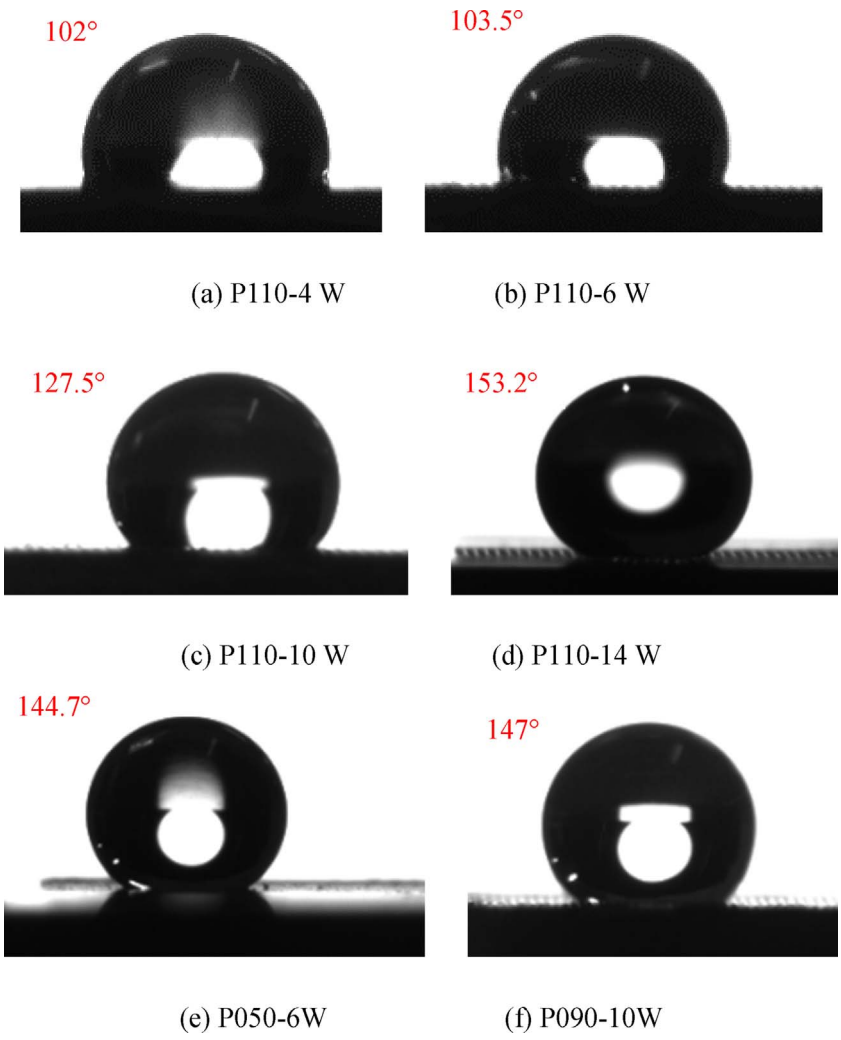

Fig. 10. Water droplet shapes for different specimens.

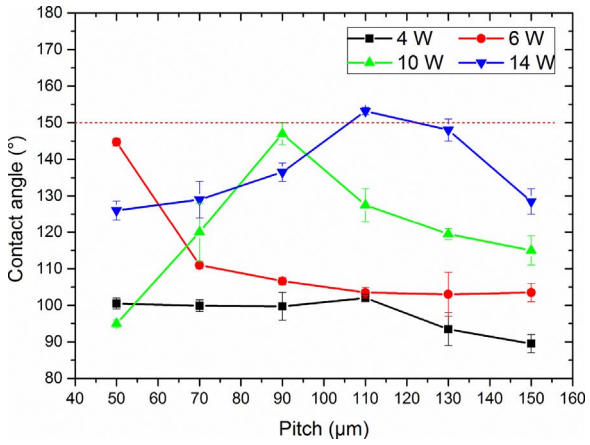

Fig. 11. Effect of laser power and pitch on hydrophobicity of laser micro structured specimens.

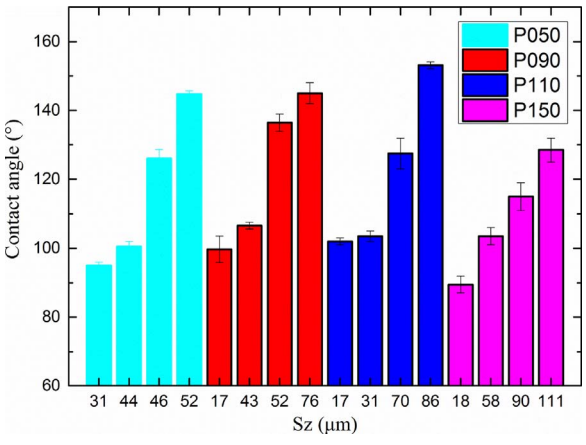

Fig. 12. Surface roughness effect on contact angle.

increases, so there are more spaces for droplet sag in. The droplet will not contact the bottom of miro holes. Thus, large Sz is an essential condition to form the stable and robust Cassie–Baxter state.

4.2.2. Comparison between experimental and theoretical values

The top three specimens which have maximum contact angle at different laser power are P050–6 W, P090–10 W and P110-14W. Their dimensions are close to predicted values. The dimensions of predicted and measured microstructures are shown in Table 5. Fig. 13 shows comparison of the predicted value of maximum contact angle with the measured value of the best three specimens. For specimen P050–6 W, the optimized b is 13.8 μm which larger than the actual value of b (23 μm) as shown in Table 5. Thus, the value of f will be larger than the designed condition. Consequently, the actual contact angle will be smaller than the predicted value as shown in Fig. 13. For the specimen P090–10 W, the actual dimension b is also larger than the predicted value as shown in Table 5, so the similar trend can be found. As for the

Table 5
Comparison between experimental and predicted values of microstructures.

		P050–6 W	P090–10 W	P110–14 W
Predicted dimensions (μm)	*a*	51.7	76.4	86
	b	13.8	31	40.8
	c	9.5	16	19.1
Actual dimensions of best specimens (μm)	*a*	52.3	75.9	87.2
	b	23.0	40.5	37.0
	c	8.2	14.5	19.8

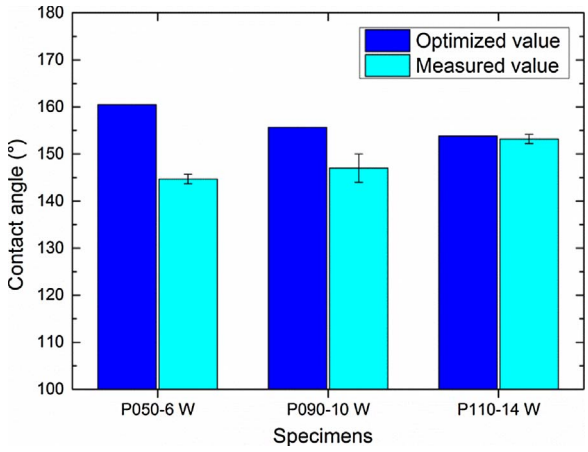

Fig. 13. Comparison between the predicted and measured contact angles.

specimen P110-14W, the actual dimension b has a small deviation (9.3%) from the predicted value, so the value of *f* will close to the ideal designed condition. Consequently, the actual contact angle at 153.2° is also very close to the predicted value of 153.8°as shown in Fig. 13.

5. Conclusions

A geometrical model for laser machined Gaussian micro holes, together with the theoretical constraints for stable Cassie-Baxter state were established in this paper for the first time to allow good understanding of the superhydrophobic mechanism and optimize the microstructure geometries. The effect of laser power, surface roughness Sz and structure pitch on the hydrophobicity of were studied through nanosecond laser machining experiments on stainless steels. The maximum contact angle (153.2°) is obtained on a microstrcutrued surface (P110-14W) with a pitch of 110 μm machined under a laser power of 14W. The conclusions can be drawn as follows:

1. The proposed geometrical model for laser machined Gaussian micro-holes can be used to accurately predict the dimensions of microstructures for maximising surface hydrophobicity.
2. The processing laser power has a significant effect on surface contact angle due to the variation of surface roughness especially the ten point height of surface topography, Sz. Under the same level of laser power, with the increase of pitch of the microstructures, the contact angle increases until it reaches its peak value. After that it drops gradually.
3. Sz is a better parameter than Sa to characterise hydrophobicity of surface with Gaussian holes. Under the same pitch of the microstructures, the contact angle will increase with the increase of Sz. Large Sz means more space for the water droplet to sag in. Thus, it is easier to form air pocket under water droplet and make the droplet have a stable Cassie-Baxter state on the specimen surface.

Acknowledgements

This research was undertaken in the context of MICROMAN project ("Process Fingerprint for Zero-defect Net-shape MICROMANufacturing", http://www.microman.mek.dtu.dk/). MICROMAN is a European Training Network supported by Horizon 2020, the EU Framework Programme for Research and Innovation (Project ID: 674801). The authors would also gratefully acknowledge the financial support from the EPSRC (EP/K018345/1) for this research. We thank the Stewart fund in the chemistry department which partially funded the purchase of the contact angle instrument.

References

[1] Wang B, Zhang Y, Shi L, Li J, Guo Z. Advances in the theory of superhydrophobic surfaces. J Mater Chem 2012;22:20112. http://dx.doi.org/10.1039/c2jm32780e.
[2] Liu K, Yao X, Jiang L. Recent developments in bio-inspired special wettability. Chem Soc Rev 2010;39:3240–55. http://dx.doi.org/10.1039/b917112f.
[3] Zhang Xiaoxue, Wang L, Levänen E. Superhydrophobic surfaces for reduction of bacterial adhesion. RCS Adv 2013;3:12003–20. http://dx.doi.org/10.1039/c3ra40497h.
[4] Privett BJ, Youn J, Hong SA, Lee J, Han J, Shin JH, et al. Antibacterial fluorinated silica colloid superhydrophobic surfaces. Langmuir 2011;27:9597–601. http://dx.doi.org/10.1021/la201801e.
[5] Qian H, Li M, Li Z, Lou Y, Huang L, Zhang D, et al. Mussel-inspired superhydrophobic surfaces with enhanced corrosion resistance and dual-action antibacterial properties. Mater Sci Eng C 2017;80:566–77. http://dx.doi.org/10.1016/j.msec.2017.07.002.
[6] Rajab F, Benson PS, Li L, et al. Picosecond laser surface micro/nano texturing of stainless Steel as a method to reduce the adhesion of bacteria. 2017.
[7] Bhushan B, Jung YC, Niemietz A, Koch K. Lotus-like biomimetic hierarchical structures developed by the self-assembly of tubular plant waxes. Langmuir 2009;25:1659–66. http://dx.doi.org/10.1021/la802491k.
[8] Feng BL, Li SH, Li YS, Li HJ, Zhang LJ, Zhai J, et al. Super-hydrophobic surfaces: from natural to artificial. Adv Mater 2002;14:1857–60. http://dx.doi.org/10.1002/adma.200290020.
[9] Zheng Y, Gao X, Jiang L. Directional adhesion of superhydrophobic butterfly wings. Soft Matter 2007;3:178. http://dx.doi.org/10.1039/b612667g.
[10] Gao X, Jiang L. Biophysics Water-repellent legs of water striders. Nature 2004;432:36. http://dx.doi.org/10.1038/432036a.
[11] Chen T, Liu H, Yang H, Yan W, Zhu W, Liu H. Biomimetic fabrication of robust self-assembly superhydrophobic surfaces with corrosion resistance properties on stainless steel substrate. RSC Adv 2016;6:43937–49. http://dx.doi.org/10.1039/C6RA06500G.
[12] Shirtcliffe NJ, McHale G, Newton MI, Chabrol G, Perry CC. Dual-scale roughness produces unusually water-repellent surfaces. Adv Mater 2004;16:1929–32. http://dx.doi.org/10.1002/adma.200400315.
[13] Kinoshita H, Ogasahara A, Fukuda Y, Ohmae N. Superhydrophobic/superhydrophilic micropatterning on a carbon nanotube film using a laser plasma-type hyperthermal atom beam facility. Carbon N Y 2010;48:4403–8. http://dx.doi.org/10.1016/j.carbon.2010.07.056.
[14] Lau KKS, Bico J, Teo KBK, Chhowalla M, Amaratunga GAJ, Milne WI, et al. Superhydrophobic carbon nanotube forests. Nano Lett 2003;3:1701–5. http://dx.doi.org/10.1021/nl034704t.
[15] Droplet CW, Mumm F, Van Helvoort ATJ, Sikorski P. Easy Route to Superhydrophobic 2009;3:2647–52.
[16] Latthe SS, Imai H, Ganesan V, Rao AV. Superhydrophobic silica films by sol-gel coprecursor method. Appl Surf Sci 2009;256:217–22. http://dx.doi.org/10.1016/j.apsusc.2009.07.113.
[17] Fürstner R, Barthlott W, Neinhuis C, Walzel P. Wetting and self-cleaning properties of artificial superhydrophobic surfaces. Langmuir 2005;21:956–61. http://dx.doi.org/10.1021/la0401011.
[18] Gleason KK, Rutledge GC, Gupta M, Ma M, Mao Y. Superhydrophobic fibers produced by electrospinning and chemical vapor deposition. US Pat Appl Publ 2007:26.
[19] Zhang X, Guo Y, Zhang P, Wu Z, Zhang Z. Superhydrophobic CuO@Cu2S nanoplate vertical arrays on copper surfaces. Mater Lett 2010;64:1200–3. http://dx.doi.org/10.1016/j.matlet.2010.02.050.
[20] Zhenyu S, Zhanqiang L, Hao S, Xianzhi Z. Prediction of contact angle for hydrophobic surface fabricated with micro-machining based on minimum Gibbs free energy. Appl Surf Sci 2016;364:597–603. http://dx.doi.org/10.1016/j.apsusc.2015.12.199.
[21] Cai Y. Hydrophobicity of pyramid structures fabricated by micro milling. World Congr Micro Nano Manuf 2017;2017.
[22] Chun DM, Ngo CV, Lee KM. Fast fabrication of superhydrophobic metallic surface using nanosecond laser texturing and low-temperature annealing. CIRP Ann – Manuf Technol 2016;65:519–22. http://dx.doi.org/10.1016/j.cirp.2016.04.019.
[23] Ta DV, Dunn A, Wasley TJ, Kay RW, Stringer J, Smith PJ, et al. Applied Surface Science Nanosecond laser textured superhydrophobic metallic surfaces and their chemical sensing applications. Appl Surf Sci 2015;357:248–54. http://dx.doi.org/10.1016/j.apsusc.2016.04.056.

[24] Long J, Pan L, Fan P, Gong D, Jiang D, Zhang H, et al. Cassie-State stability of metallic superhydrophobic surfaces with various Micro/Nanostructures produced by a femtosecond laser. Langmuir 2016;32:1065–72. http://dx.doi.org/10.1021/acs.langmuir.5b04329.
[25] Wang A, Jiang L, Li X, Xie Q, Li B, Wang Z, et al. Low-adhesive superhydrophobic surface-enhanced Raman spectroscopy substrate fabricated by femtosecond laser ablation for ultratrace molecular detection. J Mater Chem B 2017;5:777–84. http://dx.doi.org/10.1039/C6TB02629J.
[26] Martínez-Calderon M, Rodríguez A, Dias-Ponte A, Morant-Miñana MC, Gómez-Aranzadi M, Olaizola SM. Femtosecond laser fabrication of highly hydrophobic stainless steel surface with hierarchical structures fabricated by combining ordered microstructures and LIPSS. Appl Surf Sci 2016;374:81–9. http://dx.doi.org/10.1016/j.apsusc.2015.09.261.
[27] Zheng B, Jiang G, Wang W, Mei X. Fabrication of superhydrophilic or superhydrophobic self-cleaning metal surfaces using picosecond laser pulses and chemical fluorination. Radiat Eff Defects Solids 2016;171:461–73. http://dx.doi.org/10.1080/10420150.2016.1211658.
[28] Wu B, Zhou M, Li J, Ye X, Li G, Cai L. Superhydrophobic surfaces fabricated by microstructuring of stainless steel using a femtosecond laser. Appl Surf Sci 2009;256:61–6. http://dx.doi.org/10.1016/j.apsusc.2009.07.061.
[29] Jagdheesh R, García-Ballesteros JJ, Ocaña JL. One-step fabrication of near superhydrophobic aluminum surface by nanosecond laser ablation. Appl Surf Sci 2016;374:2–11. http://dx.doi.org/10.1016/j.apsusc.2015.06.104.
[30] Yang Z, Tian YL, Yang CJ, Wang FJ, Liu XP. Modification of wetting property of Inconel 718 surface by nanosecond laser texturing. Appl Surf Sci 2017;414:313–24. http://dx.doi.org/10.1016/j.apsusc.2017.04.050.
[31] Kwon MH, Shin HS, Chu CN. Fabrication of a super-hydrophobic surface on metal using laser ablation and electrodeposition. Appl Surf Sci 2014;288:222–8. http://dx.doi.org/10.1016/j.apsusc.2013.10.011.
[32] Razi S, Madanipour K, Mollabashi M. Laser surface texturing of 316L stainless steel in air and water: a method for increasing hydrophilicity via direct creation of microstructures. Opt Laser Technol 2016;80:237–46. http://dx.doi.org/10.1016/j.optlastec.2015.12.022.
[33] Razi S, Madanipour K, Mollabashi M. Improving the hydrophilicity of metallic surfaces by nanosecond pulsed laser surface modification. J Laser Appl 2015;27.4:042006. http://dx.doi.org/10.2351/1.4928290.
[34] Razi S, Mollabashi M, Madanipour K. Laser processing of metallic biomaterials: an approach for surface patterning and wettability control. EPJ Plus 2015;130:247. http://dx.doi.org/10.1140/epjp/i2015-15247-5.
[35] Trdan U, Hočevar M, Gregorčič P. Transition from superhydrophilic to superhydrophobic state of laser textured stainless steel surface and its effect on corrosion resistance. Corros Sci 2017;123:21–6. http://dx.doi.org/10.1016/j.corsci.2017.04.005.
[36] Mall A, Jelia PR, Agrawal A, Singh RK, Joshi SS. Design of arrayed micro-Structures to get super-Hydrophobic surface for single droplet and bulk flow conditions. Proc. COMSOL Conf. 2009. 2009.
[37] Butt HJ, Roisman IV, Brinkmann M, Papadopoulos P, Vollmer D, Semprebon C. Characterization of super liquid-repellent surfaces. Curr Opin Colloid Interface Sci 2014;19:343–54. http://dx.doi.org/10.1016/j.cocis.2014.04.009.
[38] Cassie BD. Wettability of porous surfaces. Trans Faraday Soc 1944:546–51. http://dx.doi.org/10.1039/tf9444000546.
[39] Graf KM, editor. Physics and chemistry of interfaces. John Wiley & Sons; 2006.
[40] https://en.wikipedia.org/wiki/Surface_tension#cite_note-s_z-7.
[41] Wenzel RN. Resistance of solid surfaces to wetting by water. Ind Eng Chem 1936;28:988–94. http://dx.doi.org/10.1021/ie50320a024.
[42] Young T. An essay on the cohesion of fluids. Trans R Soc London 1805;95:65–87. http://dx.doi.org/10.1098/rstl.1805.0005.